

GT2012-69081

## AEROACOUSTIC OPTIMIZATION FOR AXIAL FANS WITH THE LATTICE-BOLTZMANN METHOD

**Michael Stadler**  
Ninsight  
Graz, Austria

**Michael B. Schmitz**  
ebm-papst St. Georgen  
St. Georgen, Germany

**Peter Ragg**  
ebm-papst St. Georgen  
St. Georgen, Germany

**David M. Holman**  
Next Limit Technologies  
Madrid, Spain

**Ruddy Brionnaud**  
Next Limit Technologies  
Madrid, Spain

### ABSTRACT

A set of aeroacoustic optimization strategies for axial fans is presented. Their efficiency is demonstrated for small axial fans. Thereby, the generated noise could be reduced significantly while retaining or even improving the aerodynamic performance.

In particular, we discuss the following two optimization strategies in detail: Firstly, we consider the design of winglets using a parametric model for genetic optimization. The resulting winglet geometry helps to control the tip vortex over a large range of operating points, thereby reducing the generated noise. In addition, the power consumption of the fan could be reduced. Various choices of geometrical parameter sets for optimization are evaluated.

Secondly, we discuss the reduction of fan noise via contour optimized turbulators. For axial fans it is desirable to reduce sound emission across a broad operating range, not just for the design point. However, operation in off-design points may be accompanied by flow separation phenomena, which contribute predominantly to noise generation and reduce the aerodynamic performance of the fan. Turbulators can help to minimize these adverse effects. The advantages of various contoured turbulator geometries are discussed for off-design operating points.

The optimization of the above mentioned strategies was driven by aeroacoustic measurements via physical tests as well as numerical analysis based on the Lattice-Boltzmann method. The merits of either method are discussed with respect to the two optimization strategies.

### INTRODUCTION

Small axial fans are used heavily for ventilation in noise sensitive environments. For example in the IT industry, axial

fans are utilized for cooling of semiconductor equipment. Thereby, the reduction of associated noise emission has become a criterion of working ergonomics to avoid hearing loss under long term exposure. Furthermore, in the automotive industry, the introduction of automobiles propelled by electric motors will eliminate the noise due to combustion engines. Hence, other noise sources (such as fans associated with the air conditioning system) will become more apparent to the passengers. As a third example, in the design of energy efficient housing, controlled ventilation via fans utilizes heat exchangers to reduce the carbon dioxide footprint due to air conditioning. In these industries, the reduction of noise emission of axial fans has become an important marketing argument for many applications. In addition, for optimal passenger comfort, many of these applications require to control the volume flux. Hence, fan noise must be reduced also for off design behavior.

In this paper we outline two successful strategies to achieve these goals. The first strategy deals with conic winglet design to control the tip vortex. The second strategy introduces a contour optimized turbulator design that helps to reduce noise emission in particular for off design operating points. During the optimization the following cost function was minimized

$$\delta = \int_{\varphi_{\text{ref}}}^{\varphi_{\text{max}}} L_W d\varphi. \quad (1)$$

Thereby  $\varphi_{\text{ref}}$  and  $\varphi_{\text{max}}$  represent the dimensionless volume flux at the design point and at the peak volume flux, respectively.  $L_W$  represents the sound power level and  $\varphi$  is the dimensionless volume flux.

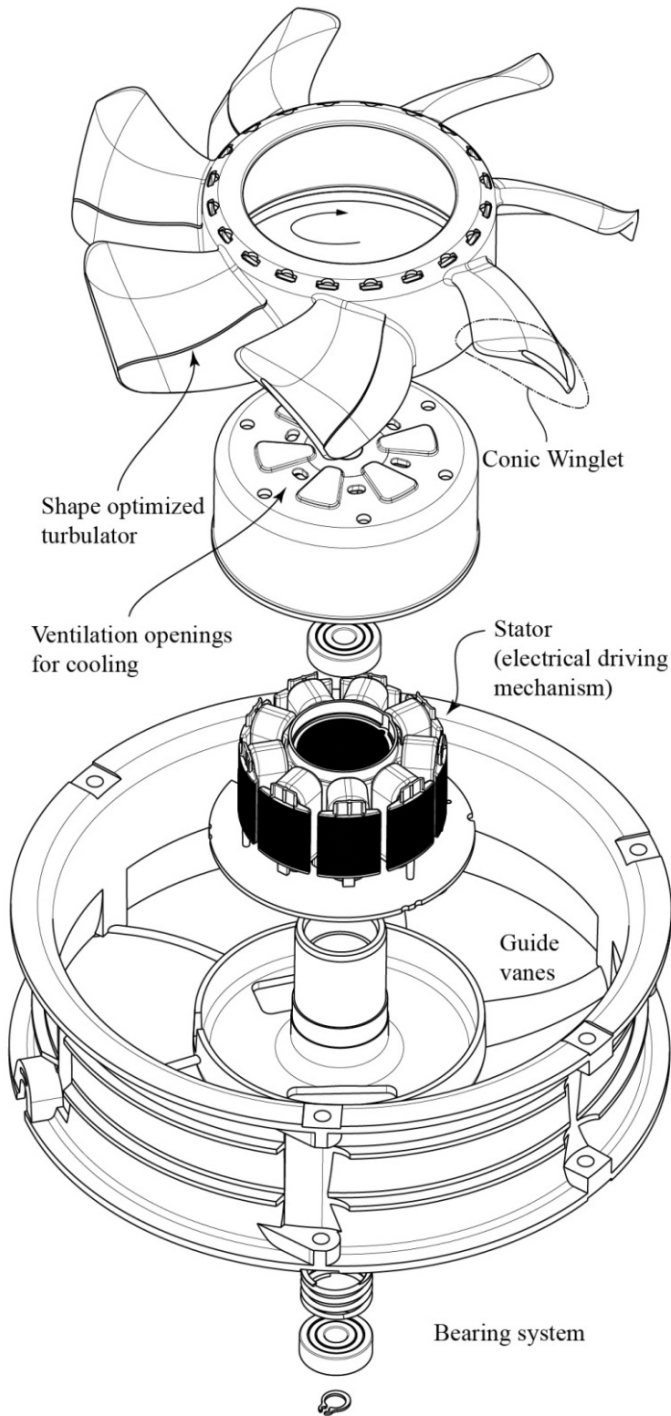


Fig. 1: Exploded view of the axial fan under investigation. The conic winglet design and the shape optimized turbulator are indicated.

The traditional development cycle for small axial fans consists of (1) designing the blade geometry, (2) performing numerical analysis to assess the aerodynamic design and (3) performing physical tests with prototypes to confirm

aerodynamic results and measure the aeroacoustic performance. However, there are several reasons why this procedure may be misleading during the aeroacoustic optimization process:

1. *Spurious noise*: the construction of physical prototypes represents time consuming manual labor that may introduce effects which have nothing to do with the aeroacoustic performance of the actual aerodynamic design. This includes noise due to imperfect rotor dynamics, eccentricity of the fan, vibration of the bearing system or noise due to secondary flow through the cooling channels of the electrical driving mechanism. The associated noise may mask the effects which we require to study and hence may render the optimization process more convoluted or even impossible.

2. *Low geometrical resolution of rapid prototyping*: the rapid prototyping process has a limited resolution of 0.1 – 0.2 mm. Turbulators represent small geometrical features that may not be accurately replicated by the rapid prototyping process. In contrast, the final product is created by injection die molding, which can replicate much finer geometrical details. Hence, the prototype model may not allow us to study certain effects associated to fine details.

Consequently we have chosen to integrate aeroacoustic numerical analysis based on direct acoustic simulation via the Lattice-Boltzmann method (LBM) into the development cycle. It helps to study effects due to geometrical details that may be too small for the rapid prototyping process and it excludes spurious noise due to secondary effects of the physical prototype. The LBM has been applied recently for similar applications in [7]-[10].

The paper is organized as follows: in the first section we discuss the conic winglet design optimization. In particular, we focus on the geometrical parameters which were utilized in the optimization process. In the second section we illustrate the contour optimized turbulator. Thereby, we discuss the several geometries to control flow separation. In the third section we outline our numerical method to drive the optimization process. We discuss tools which help to make the numerical model setup a completely automatic process. In the fourth section we present an overview of the particular Lattice-Boltzmann method used for aeroacoustic analysis. The method is also compared to similar approaches. In the fifth section we outline the experimental set-up. Finally, in the sixth section we present the results. Here we point out the advantages of the two optimization strategies by measurements of physical prototypes. Furthermore, we compare these with our numerical models to assess their reliability. All optimizations are carried out for an axial fan of diameter 150 mm, consisting of seven blades (see Fig. 1) and operating at 7200 rpm. It forms part of the new S-Force 2 family by ebm-papst.

## CONIC WINGLET DESIGN OPTIMIZATION

Aeroacoustic optimization is driven by elimination of sources in the order of their assumed intensity. The tip vortex acts as one of the dominant noise sources in axial fan design. In particular, interaction of the vortex with downstream components such as fan blades or guide vanes may lead to

vibration and generate noise. Hence, controlling the tip vortex represents a vital tool to reduce fan noise.

We have developed a parametric model of the winglet and carried out a genetic shape optimization. The goals of the optimization were specified as follows: (a) minimize the velocity in the tip vortex region and (b) prevent collision of the tip vortex with subsequent fan blades in the downstream region. The size of the gap between the shroud and the blade tip remained constant at 0.8 mm throughout the optimization.

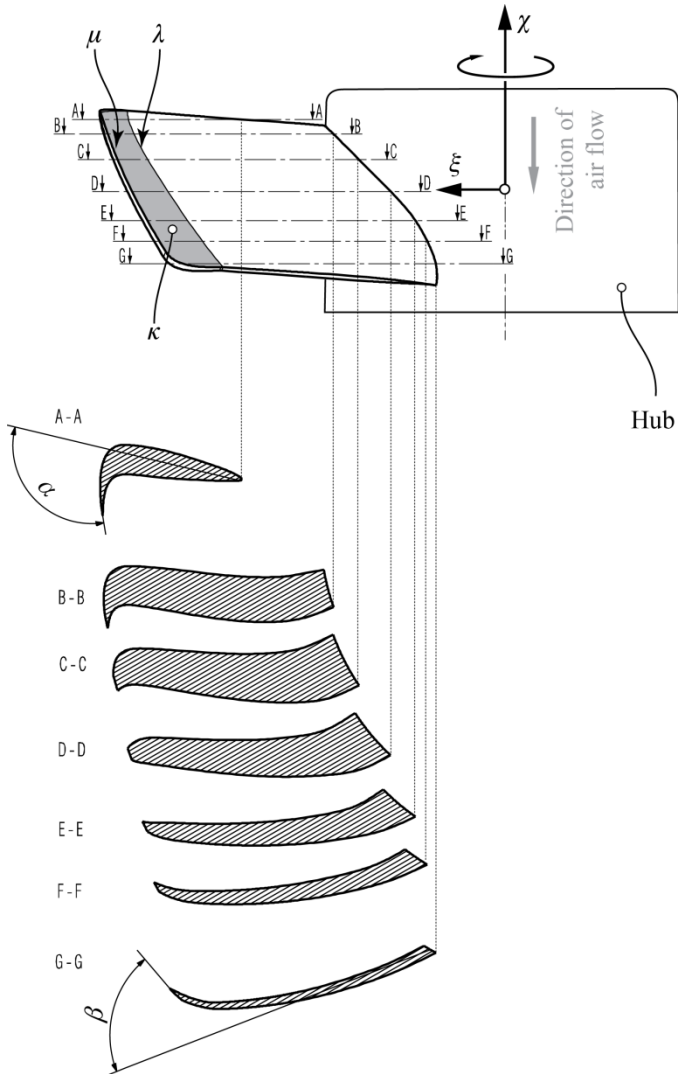


Fig. 2: Axis normal sections A-A to G-G illustrating the conic winglet geometry (only one blade shown).

**Parametric design.** Roughly speaking, the new winglet geometry represents a helical extrusion of the blade in the radial direction of the fan. In terms of parametric CAD, this arrangement is obtained by cutting the blade with a cylinder of diameter  $0.8D$  whose axis coincides with the fan axis  $\chi$  (see Fig. 2). Thereby,  $D$  represents the outer diameter of the fan. We shall denote the resulting cross section by  $\lambda$ . Subsequently, a

second cross section  $\mu$  is created by orthogonal projection of  $\lambda$  onto a cylindrical surface of diameter  $D$  and axis  $\chi$ . For successive shape optimization, it is convenient to parameterize the transformations of  $\mu$  in the following way:

- (1) rotation about the radial axis  $\xi$ ,
- (2) rotation about the fan axis  $\chi$  and
- (3) translation along  $\chi$ .

The closure of the winglet surface is obtained by a multi-section extrusion  $\kappa$  between sections  $\lambda$  and  $\mu$  (thereby enforcing  $C^1$  continuity at the interface between the original blade and  $\kappa$ , see Fig. 2).

The winglet geometry resulting from the genetic optimization process exhibits an interesting shape. It bends towards the suction side at the leading edge (angle  $\alpha$ , Fig. 2) and towards the pressure side at the trailing edge (angle  $\beta$ , Fig. 2). The detailed winglet geometry can be observed in sections A to F in Fig. 2). The curvature radius of the winglet varies along the blade. Hence, it resembles a number of generalized conic sections.

The aerodynamic as well as the aeroacoustic performance improvements due to this design will be discussed in the last section of the paper.

## CONTOUR OPTIMIZED TURBULATOR

Having reduced tip vortex intensity as one of the dominant noise sources in the previous section, we may proceed to control lower intensity noise sources in the next step. One of them is flow separation in the downstream region of the blade for off design operating points.

When air particles travel over the blade within the boundary layer, the initial part of the flow will be laminar. After a certain distance, the flow will transition from laminar to turbulent. Further downstream (at the flow separation point), the turbulent boundary layer will break down due to the large positive pressure gradient near the end of the blade. This leads to undesirable effects such as increased generation of noise and reduced cross sectional area of the flow channel. For off design operating points of the fan, the point of flow separation travels further upstream, thereby worsening the flow characteristics even more. To avoid this, we propose a turbulator design as shown in Fig. 1.

In general, turbulators are used to turn laminar flow into turbulent flow. However, turbulators can also be utilized to increase the energy of an already turbulent boundary layer, thereby moving the point of flow separation further downstream. This type of arrangement is used, for example, to avoid flow separation upstream of ailerons of commercial airliners.

In order to define the location of the turbulator, the flow across the original blade (without turbulator) is studied. To identify the location of the flow separation, the streamlines near the wall need to be analyzed. This can be done, for example, via a line integral convolution of the velocity field (which involves selectively blurring a noise image as a function of the velocity vector field) or via investigation of streamlines constrained to the elements adjacent to the wall (see Fig. 3).

The spine of the turbulator was designed as a parallel curve to the line of flow separation, which was obtained from CFD analysis. The turbulator cross section was prescribed as a simple step. To determine the optimal shape for the turbulator via genetic optimization, we have introduced two parameters: (1) offset  $\gamma$  between turbulator and line of flow separation and (2) height  $\sigma$  of the turbulator step. For the fan under investigation, the optimization yielded the following results:  $\gamma = 0.02 D$  and  $\sigma = 0.7 \text{ mm}$ .

The final fan products will be created by injection die molding. This method can easily represent sharp edges like they may appear in this turbulator design. However, for creation of the physical prototypes, selective laser sintering of polyamide was utilized (machine type EOS 390). During the winglet optimization study, this method showed excellent agreement between physical tests and CFD analysis. However, this was not the case for the turbulator under investigation. The resolution of the rapid prototyping didn't seem sufficient in order to accurately represent the stepped turbulator geometry due to its small feature size and sharp edges. In particular, in CFD analysis, the turbulator had a positive impact on static pressure of the fan. This characteristic was not observed during tests of physical prototypes. Hence, it was concluded that also acoustic measurements of physical prototypes would not deliver conclusive results. Consequently, numerical means of aeroacoustic analysis were necessary to augment the optimization process. An overview of the numerical methods used to overcome these problems is outlined in the following section.

### COMPUTATIONAL STRATEGY

Numerical simulation of the fluid dynamics was carried out mainly in Star-CCM+ V6.04 [12] using its classical Reynolds Averaged Navier Stokes (RANS) solver which is based on a polyhedral discretization scheme. Turbulent flow was resolved using the realizable two-layer  $k-\epsilon$  turbulence model as well as the integrated two-layer all  $y^+$  wall model [12]. To resolve the fine details of the geometry, a segment of the fan (i.e.  $1/7^{\text{th}}$  of the full model) was discretized by approximately 1.500.000 polyhedral and prismatic cells (see Fig. 4).

During genetic shape optimization, a large number of blade geometries needed to be analyzed. Each analysis requires a complex setup of a CFD model which represents about one hour of manual work for an experienced CFD engineer. To avoid this repetitive work, the task was automated. Therefore, a plugin software was developed that runs on top of Star CCM+ (see Fig. 5). It utilizes its highly advanced solid modeling capabilities as well as its extensive Java scripting features. The plugin software requires only the following input to analyze a fan design: (a) the blade geometry in form of a STEP file and (b) a few numerical parameters describing the shroud and hub geometry. Based on this information, the complete numerical model is set up (including the generation of fluid volumina, definition of convective boundary conditions, interfaces, mesh densities and physical models) and the CFD analysis is executed. This eliminates most of the manual labor during the

optimization process.

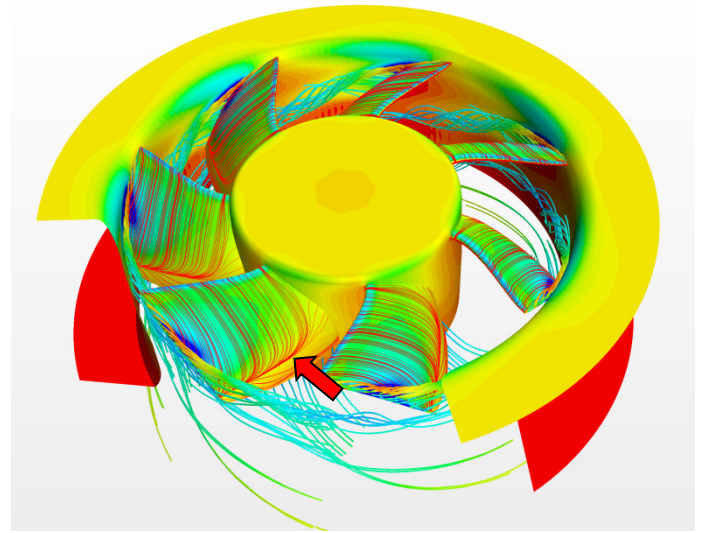


Fig. 3: Near wall streamlines of the blade without turbulator to illustrate the location of flow separation (indicated by a red arrow).

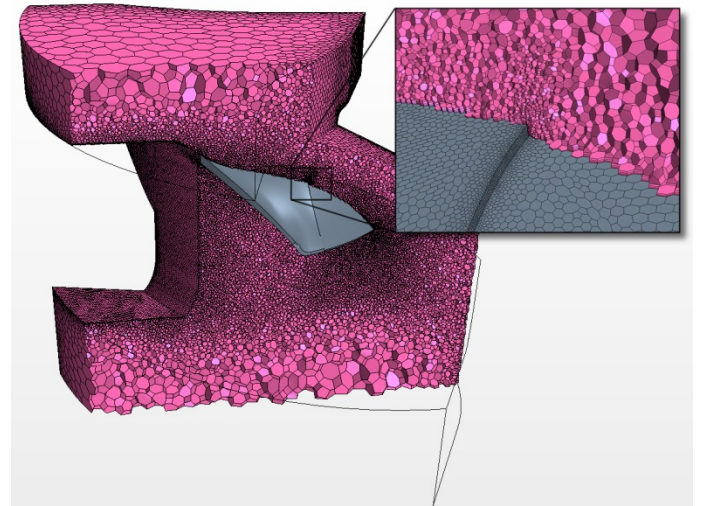


Fig. 4: Discretization of  $1/7^{\text{th}}$  of the fluid volume surrounding the blade. The inset shows a close up view of the increased mesh density near the turbulator.

For numerical analysis of the acoustic performance of the fan we used the Lattice-Boltzmann code XFlow [11]. It represents a proprietary, particle-based, meshless approach (for the geometrical model used in the simulation, see Fig. 6) which aims to solve complex problems on relatively standard computer hardware. It features a novel particle based kinetic algorithm that resolves both the Boltzmann and the compressible Navier-Stokes equations. Furthermore, it provides state-of-the-art Large Eddy Simulation (LES) modeling and

advanced non-equilibrium wall models. These features make it attractive for direct acoustic analysis within our optimization process.

Particle Method (VPM)), and (c) methods based on a mesoscopic framework (e.g. the Lattice Gas Automata (LGA) and Lattice Boltzmann Method (LBM)).

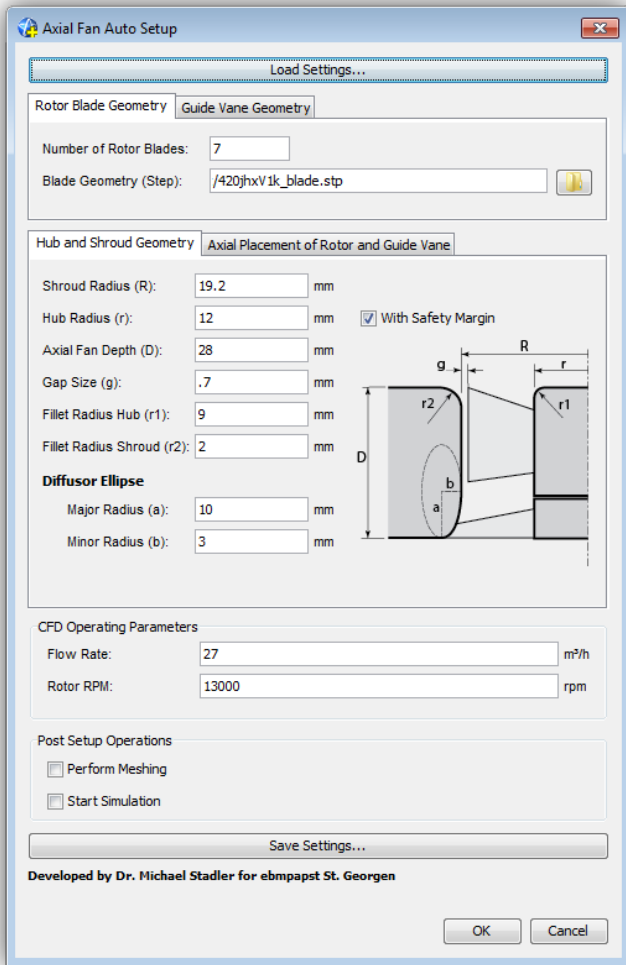


Fig. 5: Interface of the plugin software developed for Star-CCM+. It helps to automatically set up CFD simulations of an axial fan for a given set of geometrical parameters (including blade and guide vane geometry).

XFlow has been benchmarked for a number of standard fluid dynamics problems in [16]. In addition, we have performed a series of benchmarks for basic problems (cylinder in cross-flow) as well as for axial fans. These results were in good agreement with experimental data (see [17]-[19]).

**Overview of meshfree methods.** In the following we give a brief overview of meshfree methods to explain the methods used by the code. A number of meshfree numerical approaches to solve computational fluid dynamics have been published. They may be classified by the model scale as follows: (a) simulation of the fluid at the molecular level (e.g. Direct Simulation Monte-Carlo); (b) simulation at a macroscopic level (e.g. the Smoothed Particle Hydrodynamics (SPH) or Vortex

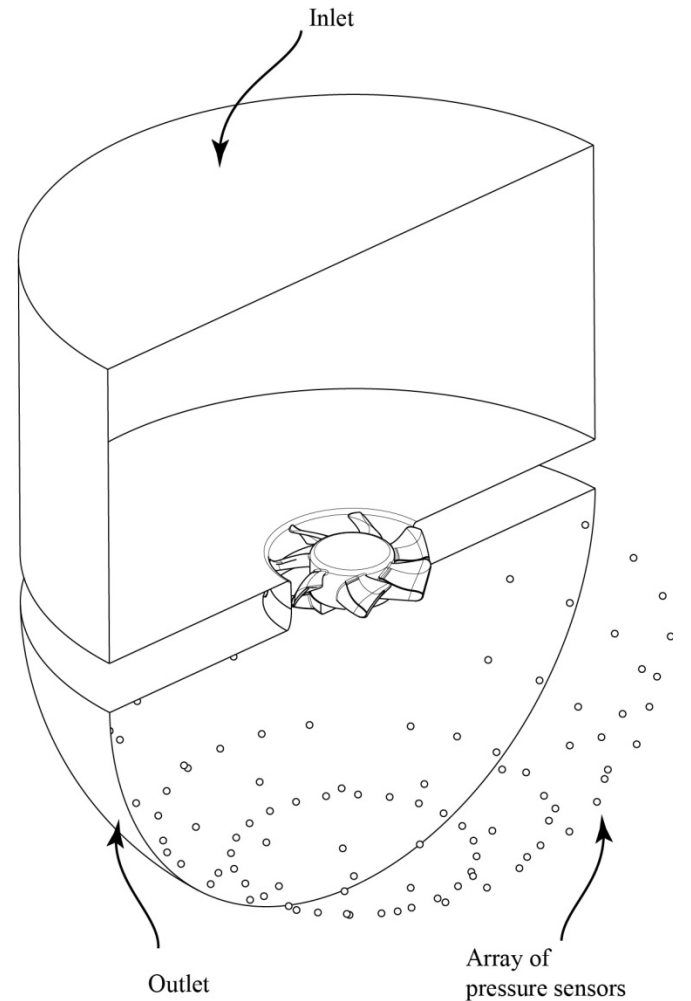


Fig. 6: Geometrical model for the Lattice Boltzmann simulation showing inlet, outlet, the fan under investigation and the array of pressure sensors (the sensors are only shown at the outlet).

Algorithms working at the molecular level are mainly used in theoretical analysis and have limited practical application. In contrast, the methods which solve macroscopic continuum equations have a wide field of application. However, they pose a number of numerical challenges. In particular, SPH methods are computationally expensive and many less advanced implementations suffer from inconsistency of the discretization scheme as well as problematic specification of boundary conditions. While VPM schemes also exhibit high computational cost, they require additional solvers (such as the boundary element method) for the pressure field, since they neglect the irrotational part of the flow.

Methods based on the mesoscopic scale (LGA and LBM) have been studied extensively (see, for example, [1]-[5], [13]

and [14]). They are attractive due to the simplicity of their computational implementation. However, the complexity associated to the analysis of emergent behavior on the macroscopic level which is controlled by laws on the mesoscopic level is less appealing. The code which was utilized here takes the main ideas behind these schemes and provides solutions to overcome most of their limitations.

**Lattice Gas Automata.** LGA schemes are simple models that allow to solve for the behavior of gases. The main idea is that the particles move discretely in a d-dimensional lattice in one of the predetermined direction at discrete times  $t=0,1,2,\dots$  and with velocity  $c_i$ ,  $i=0,\dots,b$ , also predetermined.

The simplest model is the HPP [20], introduced by Hardy, Pomeau and de Pazzis, in which the particles move in a two-dimensional square grid and in four directions. The state of an element of the lattice at instant  $t$  is given by the occupation number  $n_i(\mathbf{r},t)$ , with  $i=0,\dots,b$ , being  $n_i=1$  presence and  $n_i=0$  absence of particles moving in direction  $i$ .

The equation that governs the evolution of the system is

$$n_i(\mathbf{r} + \mathbf{c}_i \Delta t, t + \Delta t) = n_i(\mathbf{r}, t) + \Omega_i(n_1, \dots, n_b) \quad (2)$$

where  $\Omega_i$  is the collision operator, which for each previous state  $(n_1, \dots, n_b)$  computes a post-collision state  $(n_1^c, \dots, n_b^c)$  conserving the mass, linear momentum and energy;  $\mathbf{r}$  is a position in the lattice and  $\mathbf{c}_i$  a velocity.

From a statistical point of view, a system is constituted by a large number of elements which are macroscopically equivalent to the system under investigation.

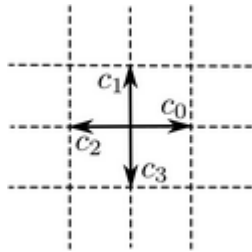


Fig. 7: Graphical representation of the model by Hardy, Pomeau and de Pazzis (HPP model).

The macroscopic density and linear momentum are:

$$\rho = \frac{1}{b} \sum_{i=1}^b n_i, \quad \rho \mathbf{v} = \frac{1}{b} \sum_{i=1}^b n_i \mathbf{c}_i \quad (3)$$

**Boltzmann's transport equation.** Boltzmann's transport equation is defined as

$$f_i(\mathbf{r} + \mathbf{c}_i \Delta t, t + \Delta t) = f_i(\mathbf{r}, t) + \Omega_i^B(f_1, \dots, f_b) \quad (4)$$

where  $f_i$  is the distribution function in the direction  $i$  and  $\Omega_i^B$  the collision operator.

From this equation and by means of the Chapman-Enskog expansion, the compressible Navier-Stokes equations can be

recovered. The Chapman-Enskog expansion shows that it is possible to design LGA schemes that recover the hydrodynamic macroscopic behavior at low Mach numbers. The main advantage of these methods is their great affinity with computers. They are easily programmed and very efficient. Some schemes have isotropy problems (do not satisfy Galilean invariance) and produce very noisy results. The main contribution of LGA schemes is that they are the precursor of the Lattice Boltzmann method.

**Lattice Boltzmann Method.** While the LGA schemes (see [21] and [22] among others) use discrete numbers to represent the state of the molecules, the Lattice Boltzmann Method (LBM) makes use of statistical distribution functions with real variables, preserving by construction the conservation of mass, linear momentum and energy.

It can be shown that if the collision operator is simplified under the Bhatnagar-Gross-Krook (BGK) approximation, the resulting scheme reproduces the hydrodynamic regime also for low Mach numbers. This operator is defined as

$$\Omega_i^{BGK} = \frac{1}{\tau} (f_i^{eq} - f_i) \quad (5)$$

where  $f_i^{eq}$  is the local equilibrium function and  $\tau$  is the relaxation characteristic time (which is related to the macroscopic viscosity).

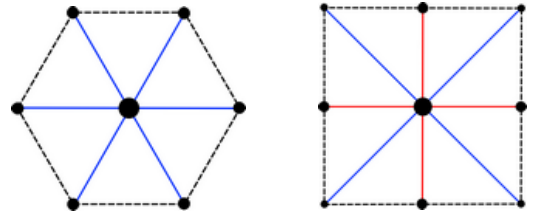


Fig. 8: Illustration of LBM schemes D2Q7 and D2Q9.

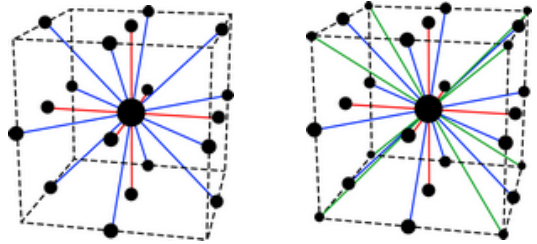


Fig. 9: Illustration of LBM schemes D3Q19 and D3Q27.

Usually, the equilibrium distribution function (see [21]) adopts the following expression:

$$f_i^{eq}(\mathbf{r}, t) = t_i \rho \left( 1 + \frac{\mathbf{c}_{i\alpha} \mathbf{v}_\alpha}{c_s^2} + \frac{\mathbf{v}_\alpha \mathbf{v}_\beta}{2c_s^2} \left( \frac{\mathbf{c}_{i\alpha} \mathbf{c}_{i\beta}}{c_s^2} - \delta_{\alpha\beta} \right) \right) \quad (6)$$

where  $c_s$  is the sound speed,  $\mathbf{v}$  the macroscopic velocity,  $\delta$  the Kronecker delta, and  $t_i$  are built preserving the isotropy in space.

LBM schemes are classified as a function of the spatial dimensions  $d$  and the number of distribution functions  $b$ , resulting in the notation  $DdQb$ . The most common schemes in two dimensions are the  $D2Q7$  and  $D2Q9$ , while in three dimensions the most used schemes are the  $D3Q13$ ,  $D3Q15$ ,  $D3Q19$  and  $D3Q27$ .

Finally, the multiscale Chapman-Enskog expansion gives the relation between the macroscopic viscosity and the relaxation parameter

$$\nu = c_s^2 \left( \tau - \frac{1}{2} \right). \quad (7)$$

For a positive viscosity, the relaxation time must be greater than 0.5. The most interesting aspect is that these schemes are able to model a wide range of viscosities  $(0, \infty)$  in an efficient way even using explicit formulations.

## EXPERIMENTAL SET-UP

From experiments we obtain fan charts and the sound power level. To facilitate testing of arbitrary configurations, a modular test set-up consisting of the following four fan components was designed: (1) casing, (2) impeller, (3) guide vanes and (4) inlet nozzle. Each of these components can be changed individually to study its particular influence on the overall performance. A typical set-up is shown in Fig. 10. The components (2)-(4) are made by rapid prototyping.

The aerodynamic test rig (see Fig. 11) is a suction side throttled facility. While the test set-up is mounted at the exit of the test rig, the air enters the rig through five tubes (see top of Fig. 11), each equipped with a flow meter. The air is conditioned with screens and gazes to ensure homogeneous flow at the fan inlet. The inherent pressure drop throughout the system is compensated for by an auxiliary fan. Fan charts are obtained by recording volume flux as well as the difference between static pressure at the inlet and ambient pressure.

The acoustic test rig (see Fig. 12) operates by throttling on the pressure side. The total sound power is computed according to ISO 10302 with ten microphones placed on a hemisphere with a diameter of 2 m. More details about the experimental set-up can be found in [15].

## RESULTS

**Aerodynamic improvements.** To illustrate the advantage of the conic winglet design, we show graphs of dimensionless pressure  $\psi = 2\Delta p_t / (\pi^2 \rho D^2 n^2)$  versus dimensionless volume flux  $\varphi = 4\dot{V} / (\pi^2 D^3 n)$  for (a) the fan without winglet (see Fig. 13, dashed line) and (b) the fan with conic winglet (see Fig. 13, solid line). Thereby,  $\Delta p_t$  is the total pressure gain,  $\rho$  is the

density of air,  $D$  represents the diameter of the fan,  $n$  is the rotary speed and  $\dot{V}$  is the volume flux. The maximum gain in dimensionless volume flux is 4% near the free blowing region.

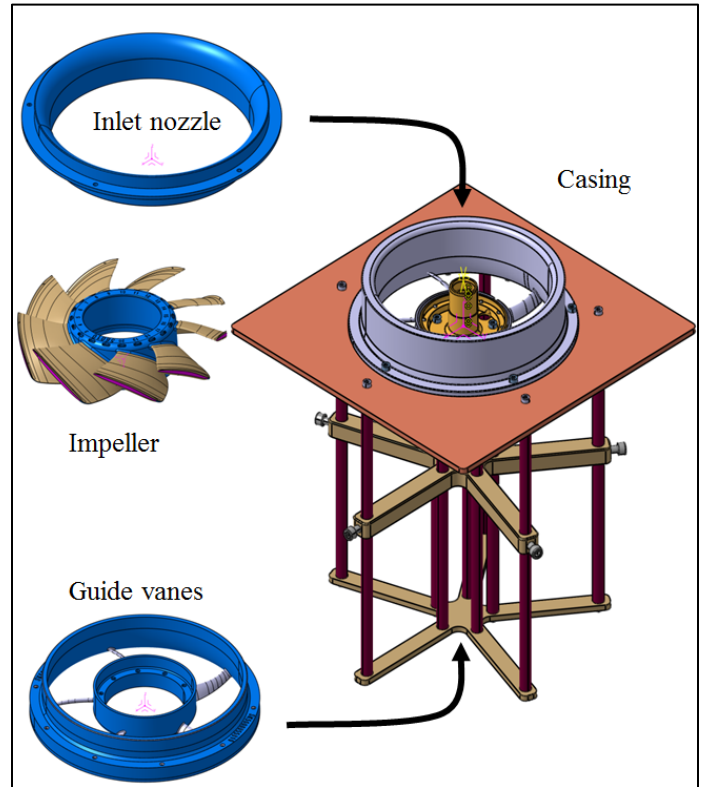


Fig. 10: Experimental set-up.

**Aeroacoustic improvements.** To show the advantage of the contour optimized turbulator, we perform tests with physical models with and without turbulator. At the design point of the fan ( $\varphi = 0.26$ , see Fig. 14), there appears no improvement in aeroacoustic noise due to the turbulator. However, for the off design region, the reduction in emitted sound power reaches about 1.0 dB ( $\varphi > 0.26$ , see Fig. 14).

In addition, we analyze the noise reduction due to the winglet design. Near the design point ( $\varphi = 0.26$ , see Fig. 14) the emitted sound power is reduced by approximately 1 dB. Further to the right in the off design behavior, the reduction in sound power reaches about 2 dB.

**Comparing acoustic simulation and physical testing.** From physical tests, the emitted sound power is available as frequency spectrum. To compare these measurements with the results from the LBM simulation, the transient static pressure is recorded at each sensor (see Fig. 15 for a sample). Via Fourier transformation, the frequency spectrum for each sensor may be obtained. The simulation was carried out with a time step of  $\Delta t = 10^{-4}$  s. Hence, by satisfying the Nyquist-Shannon sampling theorem, the frequency spectrum can be reconstructed from the transient pressure distribution up to  $f_{max} < 1/(2\Delta t) = 5000$  Hz (see Fig. 16). Clearly, the BPF up to

order three is traced out accurately. By integration over the enclosing surface, the sound power may be obtained.



Fig. 11: Aerodynamic test rig.

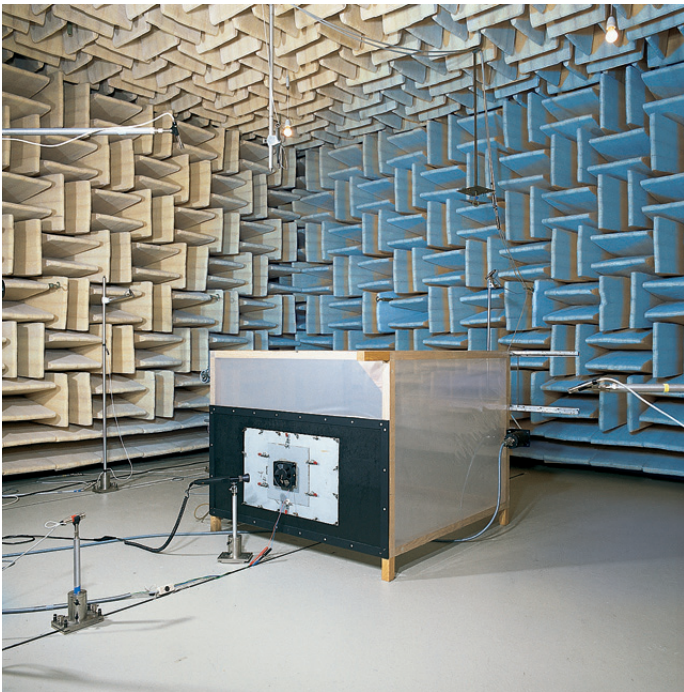


Fig. 12: Acoustic test rig.

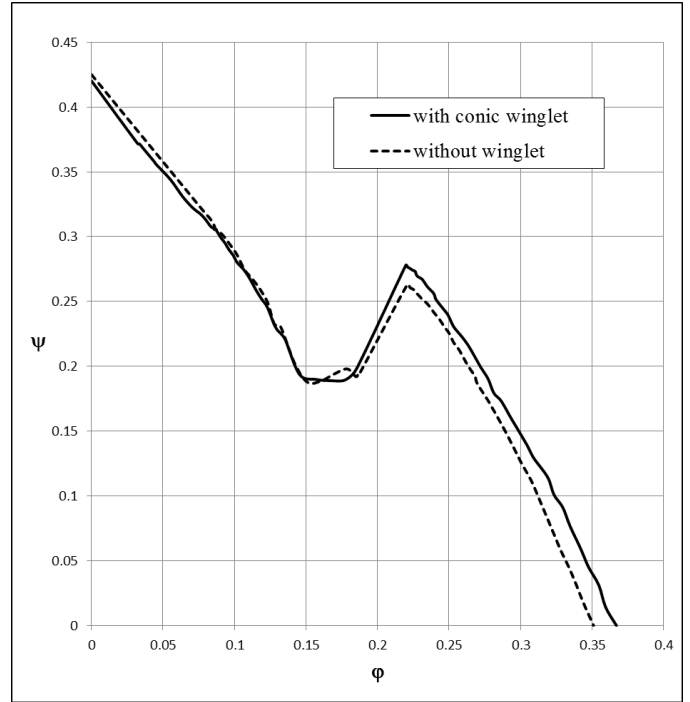


Fig. 13: Dimensionless performance curve for the fan with conic winglet (solid line) and without winglet (dashed line).

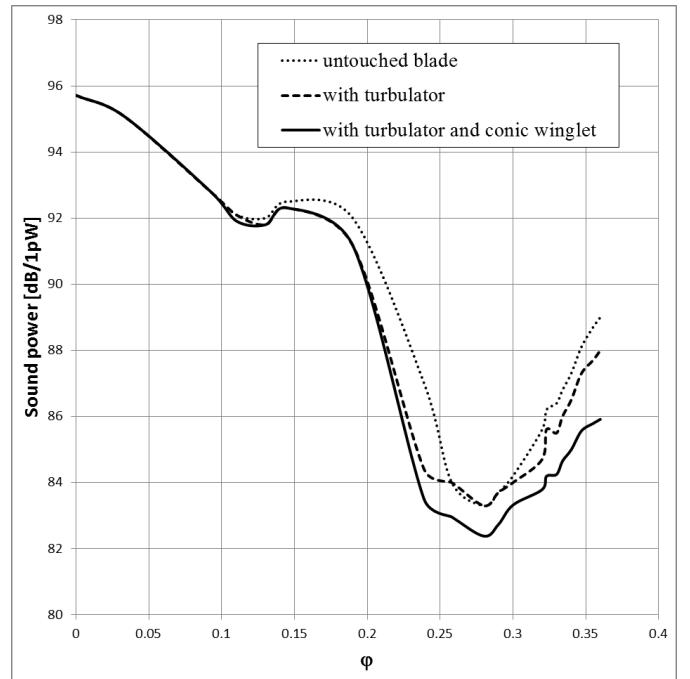


Fig. 14: Characteristic curve showing the sound power for the untouched blade (dotted curve), the blade with turbulator (dashed curve), and the blade with turbulator and conic winglet (solid curve).

To illustrate the accuracy of the numerical simulation, we show the frequency spectrum of emitted noise as 1/3-octave bands for the optimized fan design (including winglet and turbulator) operating at the design point.

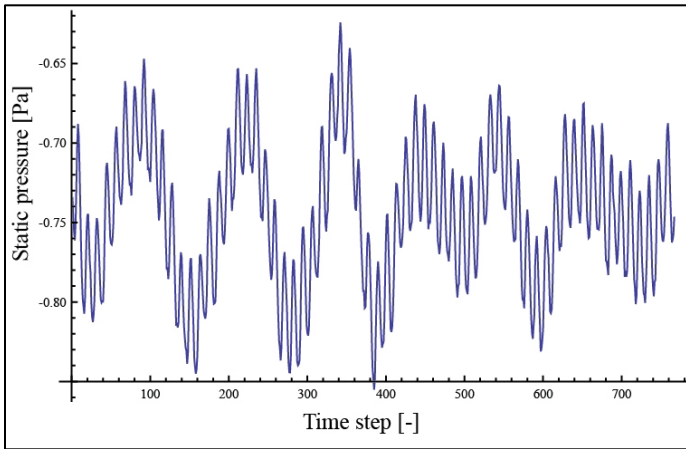


Fig. 15: Typical static pressure variation over time obtained from the Lattice-Boltzmann simulation (displayed for one of the sensors at the outlet).

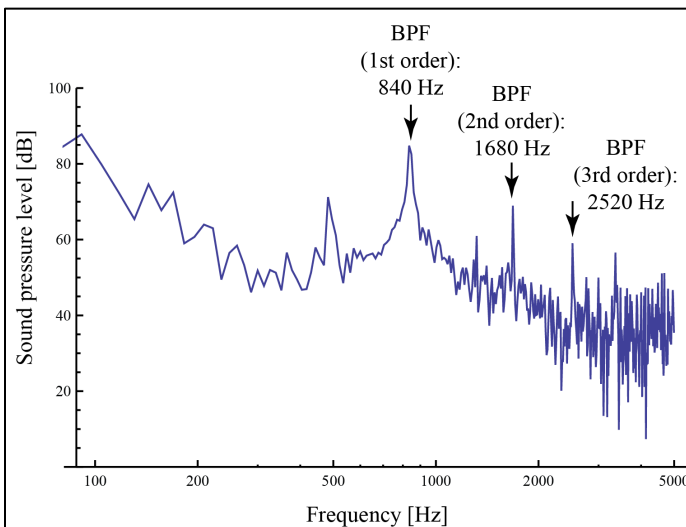


Fig. 16: Typical frequency spectrum of sound pressure level obtained from the Lattice-Boltzmann simulation for one of the sensors at the outlet. The blade passing frequencies (BPF) up to order three are indicated. The first order BPF for the fan consisting of 7 blades and operating at 7200 rpm is obtained as  $7200/60 \cdot 7 = 840$  Hz.

The overall agreement between simulation and physical test is within  $\pm 2$ dB for most of the bands (see Fig. 17). However, in the low frequency domain, the deviation is more pronounced. This situation may be mitigated by further fine tuning of simulation parameters.

There are a few interesting features to discuss: the peaks at the first and second order blade passing frequency  $BPF_1 = 7200/60 \cdot 7 = 840$  Hz and  $BPF_2 = 2 \cdot BPF_1 = 1680$  Hz are clearly visible in the frequency spectrum for both the physical test as well as for the simulation (see the 800 Hz and 1600 Hz bands in Fig. 17).

In contrast, for the physical test, another peak is observed at the rotational frequency  $RF = 7200/60 = 120$  Hz which can not be observed in the simulation. This peak is attributed to imperfect rotordynamics or eccentricity of the fan. The absence of this peak in the numerical simulation represents an advantage, since the frequency spectrum is not polluted by acoustic effects attributed to non-aerodynamic sources.

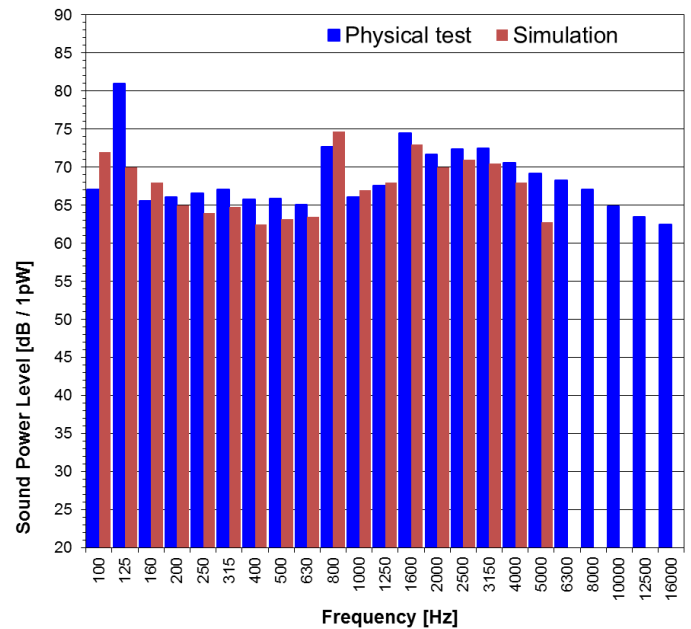


Fig. 17: Frequency spectrum of fan noise shown as 1/3-octave bands for the optimized fan (with turbulator and conic winglet) operating at the design point. Measurements for a physical test are compared with results from a numerical simulation based on direct acoustic analysis via the Lattice-Boltzmann method. The temporal resolution of the simulation was  $\Delta t = 10^{-4}$  s. Hence, in accordance with the Nyquist-Shannon sampling theorem, numerical results are limited up to a frequency of 5000 Hz. The peak for the physical test at 125 Hz is attributed to eccentricity of the fan and can therefore not be observed in the simulation.

## CONCLUSION

Two strategies have been outlined which help to reduce axial fan noise: (a) conic winglet design as well as (b) a contour optimized turbulator. The particular geometrical shape of these strategies was defined via genetic optimization of parametric geometries, physical prototypes and a standard RANS solver. Some fine geometrical details of the turbulator could not be resolved by the rapid prototyping process (which was carried

out by selective laser sintering of polyamide). Hence, the optimization process was augmented with a newly developed Lattice-Boltzmann solver. It was able to capture these fine details and give information about their aeroacoustic impact on the frequency spectrum of emitted noise. As an additional bonus, this numerical setup enables the analysis of aeroacoustic effects without spurious noise due to imperfect rotordynamics or eccentricity of the rotor. This can in turn help to accelerate the optimization process, thereby compensating for the added numerical effort.

## ACKNOWLEDGEMENTS

The authors would like to thank G. Eimer and his team for performing the experiments and ebm-papst St. Georgen GmbH for supporting this study.

## REFERENCES

- [1] Y.H. Qian, D. D'Humieres, and P. Lallemand. *Lattice BGK models for Navier-Stokes equation*. *Europhysics Letters*, 17:479, 1992.
- [2] G. McNamara and G. Zanetti. *Use of the Boltzmann equation to simulate lattice-gas automata*. *Physical Review Letters*, 61:2332, 1988.
- [3] F.J. Higuera and J. Jimenez. *Boltzmann approach to lattice gas simulations*. *Europhysics Letters*, 9:663, 1989.
- [4] S. Chen and G. Doolen. *Lattice Boltzmann method for fluid flows*. *Annual Reviews of Fluid Mechanics*, 30:329, 1998.
- [5] S. Succi. *The Lattice Boltzmann Equation for Fluid Dynamics and Beyond*. Clarendon Press, 2001.
- [6] S. Moreau, M. Sanjosé, S. Magne and M. Henner. *Unsteady Turbulent Simulations of Low-Speed Axial Fans*. 46th Symposium of Applied Aerodynamics 3AF, 2011.
- [7] M. Sanjosé, S. Moreau, M-S. Kim, F. Pérot. *Direct Simulation of Trailing-Edge Noise Generated by a Controlled Diffusion Airfoil using a Lattice-Boltzmann Method*. 7<sup>th</sup> International Symposium on Turbulence and Shear Flow Phenomena (TSFP-7), 2011.
- [8] R. E. Powell, D. Hendriana, B. Gutzeit, K. Golsch and G. Fadler, *Direct Aeroacoustic Simulation of Flow Impingement Noise in an Exhaust Opening*, SAE 2011 Noise and Vibration Conference and Exhibition, May 2011.
- [9] M. Geveler, D. Ribbrock, S. Mallach, D. Göddeke. *A Simulation Suite for Lattice-Boltzmann based Real-Time CFD Applications Exploiting Multi-Level Parallelism on modern Multi- and Many-Core Architectures*. *Journal of Computational Science*, 2:2, 2011, pp. 113-123.
- [10] S. Moreau, M. Henner, D. Casalino, J. Gullbrand, G. Iaccarino and M. Wang. *Toward the Prediction of Low-Speed Fan Noise*. Center for Turbulence Research, Proceedings of the Summer Program 2006.
- [11] XFlow user manual. Next Limit Inc. 2011.
- [12] Star CCM+ user manual. CD-Adapco, 2011.
- [13] P.L. Bhatnagar, E.P. Gross, and M. Krook. *A model for collision processes in gases*. *Phys. Rev.*, 94:511, 1954.
- [14] H. Chen, S. Chen, and W. Matthaeus. *Recovery of the Navier-Stokes equations using a lattice-gas Boltzmann method*. *Physical Review A*, 45:5339, 1992.
- [15] M.B. Schmitz, G. Eimer and H. Schmid. *Design and test of a small high performance diagonal fan*. Proceedings of ASME Turbo Expo 2011.
- [16] XFlow Validation Guide. Next Limit Inc. 2011.
- [17] V. Strouhal, "Über eine besondere Art der Tonerregung." *Annu. Phys. Chem.* Vol. 5, pp. 216-251, 1878.
- [18] H. Oertel Jr., 1990, "Wakes behind blunt bodies" *Annu. Rev. Fluid Mech.* Vol 22, pp. 539-564.
- [19] C. H. K. Williamson, 1996, "Vortex dynamics in the cylinder wake" *Annu. Rev. Fluid Mech.* Vol 28, pp. 477-539.
- [20] B. Chopard and M. Droz, *Cellular Automata Modeling of Physical Systems*, Cambridge University Press 1998.
- [21] U. Frisch, B. Hasslacher and Y. Pomeau, *Lattice-Gas Automata for the Navier-Stokes Equation*, *Phys. Rev. Lett.* 56, 1505-1508 (1986).
- [22] G. R. McNamara and G. Zanetti, *Use of the Boltzmann Equation to Simulate Lattice-Gas Automata*, *Phys. Rev. Lett.* 61, 2332-2335 (1988).